Measurement of Feedthrough and Instability Growth in Radiation-Driven Cylindrical Implosions

Warren W. Hsing and Nelson M. Hoffman
Los Alamos National Laboratory, Los Alamos, New Mexico 87545
(Received 27 December 1994)

We have performed the first radiation-driven implosions in a convergent geometry where feedthrough of the Rayleigh-Taylor instability and Bell-Plesset growth are observed. A perturbation in a dodecagon shape was machined on the outer surface of a cylindrical polystyrene shell. The shell was imploded by radiation ablation in a hohlraum at the Nova laser. Growth of the perturbation was observed at the inner surface of the shell via x-ray backlighter imaging. This method shows promise for the study of instability growth and feedthrough in converging flows. [S0031-9007(97)03162-1]

PACS numbers: 52.50.Jm, 52.25.Nr, 52.35.Py, 52.70.La

The Rayleigh-Taylor (RT) instability is of great importance in inertial confinement fusion (ICF). The instability governs the maximum allowable convergence ratio and shell aspect ratio, which in turn governs the implosion hydrodynamic efficiency. For ICF, the RT instability occurs during two phases. The first is the ablative acceleration phase where perturbations on the outer surface grow, seeded from either capsule surface nonuniformities or laser beam hot spots. The second is the deceleration phase, where the pusher-fuel interface is unstable [1] and perturbations grow from initial inner-surface nonuniformities or feedthrough via shock and acoustic wave communication from the outer surface [2,3]. Many experiments have measured RT growth during ablative acceleration in either direct [4] or indirect [5] drive and have verified the predicted stabilizing effect of mass ablation and density gradients [6]. However, few experiments have examined the role of feedthrough and the deceleration phase.

Convergent effects are also important during all phases. During the ablative acceleration phase convergence introduces a different threshold for nonlinear effects due to a decrease of perturbation wavelength in time [3] and thin shell effects [7] as well as a change in perturbation amplitude due to the combination of convergence and compressibility [8]. Feedthrough is decreased because the pusher shell thickens in time during convergence. Convergence effects are magnified during the deceleration phase [3,8–10]. There is also the potential for accelerationless Bell-Plesset growth due to convergence alone [11].

Few experiments to study convergent RT instability have been performed [12] because of the difficulty in diagnosis. Perturbations and mixing-layer widths are difficult to measure in spherical geometry due to the lack of a direct line of sight, and to the errors associated with Abel inversions in spherical geometry near the center. While perturbation growth can be indirectly inferred from time-dependent x-ray spectral line ratios in spherical implosions [13], results depend on the details of difficult atomic physics and radiative transport calculations. An indirectly driven cylindrical configuration is used in this experiment to allow diagnostic access and superior control of the shell's inner surface during target fabrication. This experiment demonstrates that quantitative RT experiments can be performed in cylindrical geometry and measures for the first time the phenomenon of feedthrough and growth in a radiation-driven target.

The experiment geometry is shown in Fig. 1. Eight 0.35 μm wavelength, 2.5 kJ, 2.2 ns Nova [14] beams are pointed symmetrically about the cylinder. A low-adiabat drive [5] is used for the main beams consisting of a low-power foot followed by a ramp to higher power, with a peak-to-foot ratio of about three. A separate beam of 2 ns duration at 0.53 μm wavelength is used to irradiate a 2 mm diam silver disk to create an x-ray backlighter of photon energy $\sim 3-3.6$ keV.

The central 400 μm long region of the cylinder has perturbations machined on the outer surface in a dodecagon shape (fundamental mode number $m = 12$), giving a peak-to-valley amplitude of 9 μm. In the central region, the shell wall is 45 μm thick, with 260 μm outer radius. A 4-μm-thick, 160-μm-long dichlorostyrene ($C_8H_6Cl_2$)

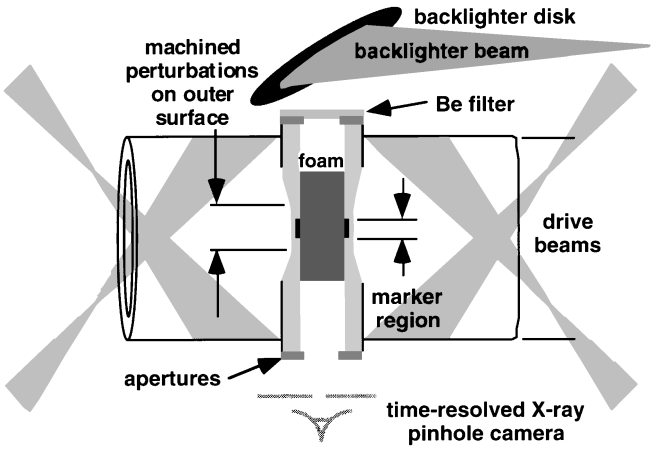

FIG. 1. View of the experimental geometry. The hohlraum has a length of 2750 μm, a diameter of 1600 μm, and a laser entrance hole diameter of 1280 μm.

 0031-9007/97/78(20)/3876(4)$10.00

belt is placed around the center of the cylindrical shell, flush with the shell's inner surface. The belt serves as a marker layer since it is opaque to the x-ray backlighter, whereas the polystyrene cylinder is relatively transparent. Although it is the marker layer which is most clearly evident in the time-resolved pinhole camera diagnostic, at late time the neighboring compressed polystyrene becomes somewhat opaue, according to calculations. While the marker layer has an initial density higher than the unchlorinated polystyrene (1.4 g/cm^3 versus 1.0 g/cm^3), calculations show that expansion of the marker layer from x-ray preheat reduces the density to below the unchlorinated polystyrene during the ablative acceleration phase. [This expansion can be seen in Fig. 4(a) as an increase in the calculated distance between the inside and outside of the marker layer.] Thus the outer marker layer-polystyrene interface is expected to be Rayleigh-Taylor stable. A 60 mg/cm^3 microcellular polystyrene foam with cell size $\sim 2-3$ μm is placed inside the shell to provide a back pressure as the cylinder implodes. On each end of the cylinder, a 400 μm diam circular aperture is placed concentric with the cylinder axis. These apertures provide a centering fiducial for each frame on the pinhole camera. The cylinder is viewed along its axis with a time-resolved gated x-ray pinhole camera (GXI) [15]. A 4×4 pinhole array with pinhole diameters of ~ 7 μm allowed 16 images spaced ~ 55 ps apart to be projected onto four microchannel plate strip lines with a magnification of 12.

Figure 2 shows twelve images of an implosion with the initially perturbed surface as described. The times are shown with respect to the start of the laser pulse. The perturbation amplitude grows in time and the wavelength decreases as the radius decreases. According to calculations the ablation front does not reach the marker layer during the implosion. Hence the existence of an observed $m = 12$ feature is due to feedthrough of the initial perturbation to the marker layer. The tips of the dodecagon have grown into spikes. An image of an unperturbed cylindrical implosion taken under identical conditions to a perturbed implosion shows an absence of $m = 12$ perturbations, demonstrating that the initial perturbations caused the observed feedthrough.

In the perturbed image, a contour is identified at the inner and outer edges of the marker layer at the $\sim 50\%$ exposure level and the Fourier coefficients a_m and b_m are determined. The contour is expressed as $r(\theta) = \frac{1}{2}a_0 + \sum_m (a_m \cos m\theta + b_m \sin m\theta)$. The result is shown in Fig. 3 for the Fourier amplitude $\sqrt{a_m^2 + b_m^2}$ (μm) for the outer edge as a function of mode number m for $t = 2.11$ ns. The fundamental mode 12 amplitude has grown from an initial value of 3.5 to 10 μm, a factor of 2.9 compared to its initial value. The perturbations are observed to conserve mode number during the implosion, despite the observation that one side of the target has imploded closer to the center than the other side. (This is due to a combination of power imbalance and target nonuniformity.) Sources of error include the choice of center, contour level, and instrumental resolution and instrumental noise. There are also local maxima at modes 1, 4, and 8. The mode 4 maximum is due to the discrete number of drive beams, which provides an illumination asymmetry. The mode 8 maximum is the result of coupling of the mode 4 drive asymmetry to the mode 12 target perturbations.

The observed perturbation growth is consistent with estimates made from the modified Takabe relation [6] $\gamma = \sqrt{kg/(1 + kL)} - \beta k v_a$, where γ is the growth rate of an ablation-surface perturbation with wave number k, under an acceleration g, in the presence of a density-gradient scale length L, and ablation velocity $v_a = \dot{m}/\rho_{\max}$, where $\rho_{\max}$ is the maximum mass density near the ablation

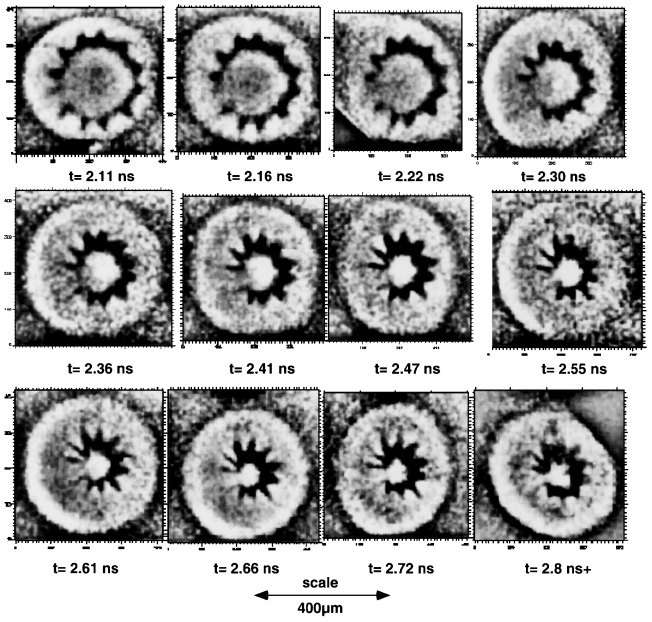

FIG. 2. A sequence of gated x-ray images of the cylindrical backlit implosion. Emission appears on center at 2.30 ns, when the shock wave converges at the origin.

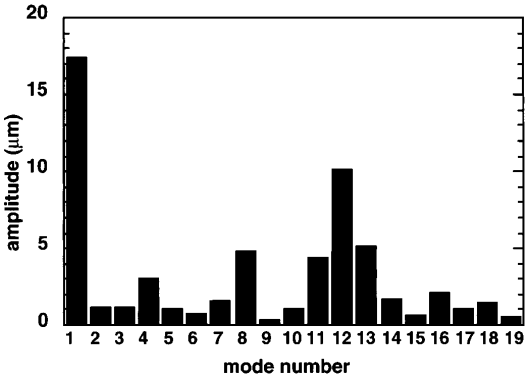

FIG. 3. Fourier amplitudes as a function of mode number taken from a contour of the outer edge of the marker layer at 2.11 ns.

front and $\dot{m}$ is the mass ablation rate. The coefficient β is an adjustable parameter ~ 0.5–4 [5]. The expression $\exp(\int \gamma\, dt)$ is numerically integrated using HYADES [16], a one-dimensional radiation-hydrodynamic code, to obtain the growth rate during the acceleration. Assuming that the perturbation amplitude at the marker layer is equal to the amplitude at the ablation front reduced by the feedthrough factor $e^{-k\Delta r}$, where Δr is the distance between the ablation front and marker layer, the ablation front amplitude is inferred from the measured amplitude at the marker layer simply by multiplying by $e^{k\Delta r}$. From the simulations, $\Delta r \sim 9\ \mu$m, $k \sim 0.087\ \mu\text{m}^{-1}$, resulting in a reciprocal feedthrough factor of 2.2. The observed growth factor is matched using a value of $\beta \sim 0.7$.

The coefficient $a_0/2$ which represents the average radius is plotted as a function of time in Fig. 4(a) for the inner and outer edges of the marker layer, along with the convergence ratio of the outer edge of the marker layer. The implosion trajectory is consistent with a 190-eV peak brightness temperature input into a calculation with HYADES. A measured non-Planckian spectral profile typical of gold hohlraum emission which includes M-shell gold emission components [5] is used. In Fig. 4(b), the time-dependent modal amplitudes of the $m = 4$ and $m = 12$ modes for the outer edge of the marker layer are shown as a function of time. The quadrature sum $\sqrt{a_{11}^2 + b_{11}^2 + a_{12}^2 + b_{12}^2 + a_{13}^2 + b_{13}^2}$ represents the mode

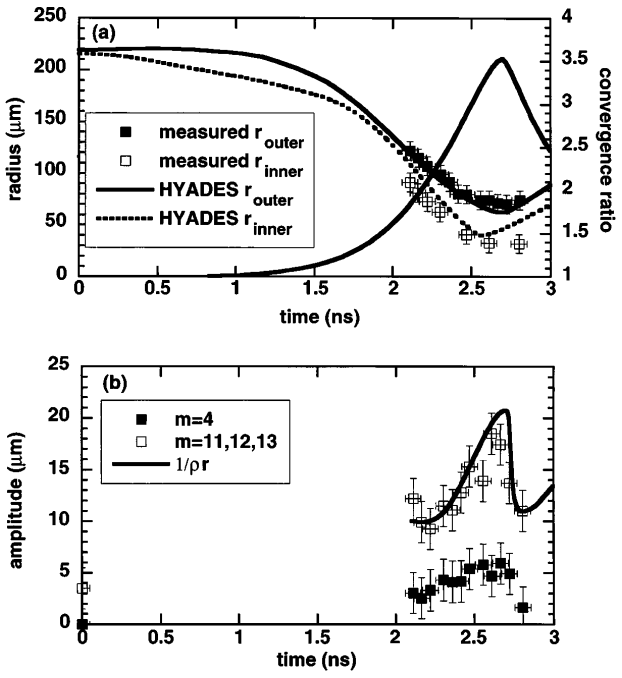

FIG. 4. (a) The measured outer and inner radius of the marker layer (Fourier coefficients $a_0/2$) as a function of time compared to the trajectories from a HYADES calculation. The convergence ratio of the outer marker layer edge is also shown. (b) The Fourier modal amplitudes $\sqrt{a_4^2 + b_4^2}$ and $\sqrt{a_{11}^2 + b_{11}^2 + a_{12}^2 + b_{12}^2 + a_{13}^2 + b_{13}^2}$ as a function of time. The value $1/\rho r$ is superposed.

12 amplitude, since errors in the choice of center can shift the modal amplitude by ± 1 mode.

The instability measured at the outer edge of the marker layer should also cause feedthrough to the inside edge of the marker layer. At $t = 2.30$ ns, the Fourier analysis of the outer edge gives a 11.5 μm amplitude, and for the inner edge, a 2 μm $m = 12$ amplitude, or an attenuation of 0.18. Using $k = 0.12\ \mu\text{m}^{-1}$ and a marker layer thickness from the simulations of 17 μm, results in an attenuation of $e^{-k\Delta r} = 0.14$, consistent with the measurement.

For $t > 2$ ns, the outer marker layer interface decelerates and is Rayleigh-Taylor stable. The mode 12 amplitude grows from $\sim 10\ \mu$m to $\sim 18\ \mu$m. This is due to Bell-Plesset instability, which includes a purely geometrical effect. The growth can be estimated by considering a compressible fluid without acceleration or almost equivalently, a low Atwood number interface ($A \sim 0.15$). The amplitude in cylindrical geometry varies as $\sim 1/\rho r$ [11]. Using values of ρ and r in the center of the marker layer from the 1D simulation and normalizing the amplitude to 10 μm at 2.11 ns, the resultant growth is plotted in Fig. 4(b). From $t = 2.0$ ns to $t = 2.3$ ns (convergence ratio of 1.7 to 2.7 for the marker layer), there is little growth, because the effect of compressibility offsets the effect of convergence; i.e., ρ increases as r decreases. From $t = 2.3$ ns to $t = 2.7$ ns (convergence ratio 2.7 to 3.5), the marker layer behaves incompressibly; ρ is constant as r decreases and significant growth occurs with the modal amplitude varying as $\sim 1/r$. During expansion ($t > 2.7$ ns), the marker layer is compressed by an outward-going shock, the density increases, and the perturbation amplitude decreases. These results imply that convergence and compressibility strongly affect perturbation growth during the deceleration and stagnation phase.

The ablation front amplitude has become nonlinear in this experiment. The threshold occurs nominally at $A/\lambda \sim 0.1$, where A is the perturbation amplitude, although in simulations it depends both on the initial amplitude and shell thickness [7]. From 2D simulations with LASNEX [17], the departure from linearity occurs at $t > 1.7$ ns. At that time, $\exp(\int \gamma\, dt) = 5.1$, or 80% of the growth if it was linear during the entire experiment. Thus nonlinearity is not a dominant effect in this experiment. The perturbation was initialized in its linear regime ($A/\lambda = 0.026$). At time $t = 2.11$ ns, $A/\lambda = 0.18$, above the nominal threshold for linearity. Without convergence, the mode 12 would have remained in the linear regime ($A/\lambda = 10/136 = 0.07$). Observation of a large mode 8 amplitude $\sim 5\ \mu$m implies that the mode 12 has become nonlinear and coupled to the mode 4, which is still in the linear regime. The reduction of the growth rate due to thin shell effects is $\sqrt{(1 - \sigma)/[1 + \sigma \coth(kh)]}$, where $\sigma = \rho/\rho'$, ρ is the mass density and h is the shell thickness [18]. From the simulations, $kh > 2$, $\sigma < 0.05$, resulting in a 2% bound on the reduction in growth rate due to thin shell effects. The effect of feedthrough at later time dominates the

effect of shock induced growth of the marker perturbation. This can be estimated by considering the creation of a perturbed shock from the ablation front, the propagation of the shock to the marker layer, and the subsequent growth of the imprinted perturbation on the marker layer [19]. This phenomenon is subtly different from the Richtmyer-Meshkov instability [20]. Using values from the simulation for the second shock, which is the predominant effect, and an initial amplitude of 3.5 μm, results in an upper limit for the marker layer amplitude of 0.3 μm at 2.1 nsec due to shock induced growth. This is 3% of the observed mode 12 amplitude at that time; thus shock induced growth is negligible compared to the observed growth.

In conclusion, radiation-driven cylindrical implosions have been performed and the RT instability feedthrough from the ablation surface to the inner surface, coupling of drive asymmetries with surface modes, and the presence of Bell-Plesset growth during the stagnation phase have been observed. This experiment shows the potential for new quantitative studies of RT instability in convergent geometry: convergence effects in Rayleigh-Taylor growth using multiple marker layers to simultaneously measure ablation front growth, phase reversal, and feedthrough in space and time, mode coupling of illumination asymmetry with surface modes which is predicted to cause the reduction of neutron yields from 1D simulations of capsule implosions [21], convergent growth of low-initial-amplitude single modes with high growth factors on the inner surface during the deceleration phase of an implosion, and expansion phase trajectory measurements. With higher resolution, studies of the stagnation phase and inner-surface breakup may be possible.

The authors would like to thank A. Hauer, L. Suter, and S. Haan for suggestions, the target fabrication team at LANL, J. Beck, G. Magelssen, and N. Delamater for calculations, C. Barnes, T. Dittrich, B. Hammel, B. Remington, and O. Landen for useful discussions, technicians for help with the GXI, the NOVA operations crew for their assistance, D. Phillion for the use of his analysis code, and J. Mack for his support. This work was supported by the U.S. D.O.E. under Contract No. W-7405-ENG-36.

[1] J. D. Lindl and W. C. Mead, Phys. Rev. Lett. **34**, 1273 (1975); S. E. Bodner, Phys. Rev. Lett. **33**, 761 (1974); D. B. Henderson, R. L. McCrory, and R. L. Morse, Phys. Rev. Lett. **33**, 205 (1974).

[2] K. Mikaelian, Phys. Rev. A **42**, 4944 (1990); K. Mikaelian, Phys. Rev. A **31**, 410 (1985).

[3] S. W. Haan, Phys. Rev. A **39**, 5812 (1989).

[4] A. J. Cole *et al.,* Nature (London) **299**, 329 (1982); M. Desselberger and O. Willi, Phys. Fluids B **5**, 896 (1993); J. Grun *et al.,* Phys. Rev. Lett. **58**, 2672 (1987); H. Nishimura *et al.,* Phys. Fluids **31**, 2875 (1988); A. P. Fews, M. J. Lamb, and M. Savage, Laser Part. Beams **11**, 257 (1993); S. G. Glendinning *et al.,* Phys. Rev. Lett. **69**, 1201 (1992).

[5] B. A. Remington *et al.,* Phys. Fluids B **5**, 2589 (1993); B. A. Remington *et al.,* Phys. Fluids B **4**, 967 (1992); B. A. Remington *et al.,* Phys. Rev. Lett. **67**, 3259 (1991); S. V. Weber *et al.,* Phys. Plasmas **1**, 3652 (1994).

[6] H. Takabe, L. Montierth, and R. L. Morse, Phys. Fluids **26**, 2299 (1983); S. E. Bodner, Phys. Rev. Lett. **33**, 761 (1974); D. H. Munro, Phys. Rev. A **38**, 11 433 (1988).

[7] G. R. Baker *et al.,* J. Fluid Mech. **178**, 161 (1987); C. P. Verdon *et al.,* Phys. Fluids **25**, 1653 (1982); R. L. McCrory *et al.,* Phys. Rev. Lett. **46**, 336 (1981).

[8] F. Hattori, H. Takabe, and K. Mima, Phys. Fluids **29**, 1719 (1986).

[9] R. P. J. Town and A. R. Bell, Phys. Rev. Lett. **67**, 1863 (1991).

[10] H. Sakagami and K. Nishihara, Phys. Rev. Lett. **65**, 432 (1990); H. Sakagami and K. Nishihara, Phys. Fluids B **2**, 2715 (1990).

[11] G. I. Bell, Los Alamos Scientific Laboratory Report No. LA-1321, 1951; M. S. Plesset, J. Appl. Phys. **25**, 96 (1954); H. N. Fisher, Los Alamos National Laboratory Memorandum No. X-1(5/82)22, 1982.

[12] M. A. Sweeney and F. C. Perry, J. Appl. Phys. **52**, 4487 (1981); J. S. Wark *et al.,* Appl. Phys. Lett. **48**, 969 (1986); H. Nishimura *et al.,* Phys. Fluids **31**, 2875 (1988).

[13] T. R. Dittrich *et al.,* Phys. Rev. Lett. **73**, 2324 (1994).

[14] E. M. Campbell, Laser Part. Beams **9**, 209 (1991).

[15] J. D. Kilkenny *et al.,* Rev. Sci. Instrum. **59**, 1793 (1988); O. L. Landen *et al.,* in *Ultra-high and High-Speed Photography, Videography, and Photonics 1993*, edited by P. W. Roehrenbecks (SPIE, San Diego, 1993), Vol. 2002, pp. 2–12.

[16] J. T. Larsen and S. M. Lane, J. Quant. Spectrosc. Radiat. Transfer **51**, 179 (1994).

[17] G. B. Zimmerman and W. L. Kruer, Comments Plasma Phys. **2**, 85 (1975).

[18] L. D. Landau and E. M. Lifshitz, *Fluid Mechanics* (Pergamon, New York, 1987), 2nd ed.

[19] R. Ishizaki *et al.,* Phys. Rev. E **53**, 5592 (1996); K. Nishihara and R. Ishizaki, Bull. Am. Phys. Soc. **41**, 1558 (1996); T. Endo *et al.,* Phys. Rev. Lett. **74**, 3608 (1995).

[20] R. D. Richtmyer, Commun. Pure Appl. Math. **13**, 297 (1960).

[21] M. M. Marinak *et al.,* Phys. Plasmas **3**, 2070 (1996).